Symmetry breaking in two dimensions on ultrafast timescales

Alireza Valizadeh [1,2] Patrick Dillmann,[3] and Peter Keim [4,*]

[1]*Max-Planck-Institute for Dynamics and Self-Organization, 37077 Göttingen, Germany*

[2]*Institute for the Dynamics of Complex Systems, University of Göttingen, 37077 Göttingen, Germany*

[3]*Department of Physics, University of Konstanz, D-78467 Konstanz, Germany*

[4]*Institute for Experimental Physics of Condensed Matter, Heinrich-Heine-Universität Düsseldorf, 40225 Düsseldorf, Germany*

(Received 3 February 2025; accepted 19 January 2026; published 10 February 2026)

The melting of two-dimensional monocrystals is described within the celebrated Kosterlitz-Thouless-Halperin-Nelson-Young scenario by the dissociation of topological defects. It describes the screening of elasticity due to thermally activated topological defects until shear elasticity disappears. As a well-defined continuous phase transition, freezing and melting should be reversible and independent of history. However, this is not the case: Cooling an isotropic two-dimensional fluid at a finite but nonzero rate does not result in monocrystals. The symmetry cannot be broken globally but only locally within Einstein's event horizon: The slowing down of critical fluctuations forces the system to fall out of equilibrium, resulting in finite-sized domains with a uniform order parameter. For linear cooling rates, the domain size is described by the Kibble-Zurek mechanism, originally developed for defect formation in the primordial Higgs field shortly after the Big Bang. The size of the domains is a function of the so-called fallout time, the time when the ensemble becomes nonergodic. In the present manuscript, we go beyond the Kibble-Zurek picture and investigate the limit of the deepest quench on a colloidal monolayer. We resolve the time dependence of structure formation for (local) symmetry breaking when the fallout time is effectively set to zero. However, when quenching instantaneously to various temperatures below the melting point—either deep in the crystalline phase or close to the transition—we find universal behavior if the timescale is rescaled properly.

DOI: 10.1103/rmd6-ll3b

I. INTRODUCTION

The glass transition temperature depends on the cooling rate and shows memory effects; thus, it does not mediate between well-defined thermodynamic states in the classical sense [1–4]. This is different for phase transitions where melting and freezing are assumed to be reversible. However, this is only partly true for discontinuous (first-order) phase transitions, where a nucleation barrier has to be overcome. For careful cooling/heating and very clean ensembles (free of seeds leading to heterogeneous nucleation), the systems can be supercooled or overheated, indicating some hysteresis in transition temperatures. The maximal width of the hysteretic region ranges up to the spinodal, where the slope of, e.g., the van der Waals curve becomes negative and phase separation must set in [5]. Note that it is *a priori* not clear whether an ensemble, which in equilibrium shows continuous behavior, may experience a nucleation barrier during transformation when being out of equilibrium: The nondegenerate minimum (true vacuum state) of the Mexican-hat free-energy potential in the high-symmetry phase and the degenerate minima of the symmetry-broken phase—and especially the smooth transition from one to the other—are only well defined in equilibrium.

For continuous (second-order) phase transitions in equilibrium, nucleation barriers do not exist, ruling out any hysteresis of the transition. At the transition temperature, the free-energy densities of the high- and low-temperature phases are identical, eliminating any driving force for phase separation. Consequently, there is *a priori* no reason to expect freezing and melting not to be completely reversible. However, critical fluctuations of the order parameter dictate the behavior of the ensemble, and timescales become important. A famous example is the Ising model in two dimensions (2D) [6], which is, besides the 2D *XY* model and the 2D particle system described in Kosterlitz-Thouless-Halperin-Nelson-Young theory [7–11], one of the rare examples with an analytic solution of the transition temperature T_c. Above T_c, magnetic moments randomly point upward and downward; the ensemble is homogeneous and isotropic. Below T_c, the magnetic moments organize to align parallel, and a macroscopic magnetization builds up. This magnetization can be taken as an order parameter, and the symmetry of the ensemble is broken. Whether the magnetization points upward or downward is a matter of chance—part of the story why this phenomenon is called *spontaneous* symmetry breaking. Typically, it is assumed that by crossing T_c from the high-temperature to the low-temperature phase, the symmetry switches globally. However, taking timescales into account, this cannot be the truth in

*Contact author: peter.keim@uni-duesseldorf.de

the thermodynamic limit: In infinitely large ensembles, only regions that are connected by causality can have the same order parameter after symmetry breaking. Regions that are separated by a distance larger than the speed of light times the time after crossing T_c (defining an event horizon) cannot necessarily acquire the same order parameter. The symmetry is broken only locally, and the order parameter can be uniform only within the event horizon: Melting and freezing are not reciprocal in the thermodynamic limit.

This idea was first discussed by Tom Kibble [12–14] for symmetry breaking of the very first field shortly after the Big Bang. This two-component scalar field is nowadays often named the inflaton. Topological defects like grain boundaries, strings, and monopoles should be incorporated as leftovers of the high-symmetry field in the symmetry-broken stage. Zel'dovich, for example, calculated optical properties of grain boundaries within the Higgs field for detecting their traces within the electromagnetic background radiation in the Universe [15]. Up to now, such defects have never been observed, which is one of the reasons (besides the flatness of space-time of the Universe and the overall very isotropic cosmic microwave background) for postulating *inflationary* Big Bang models: During the exponentially fast growth of the very early Universe, all defects have been pushed beyond the event horizon.

Wojciech Zurek [16–18] applied similar ideas to another two-component, but complex, field, namely, the macroscopic wave function of superfluid helium. In this three-dimensional (3D) system with a two-component ($2N$) order parameter, the most natural topological defects are strings, given by the vortices of the wave function with a normal-fluid core. In condensed matter, the maximal signal velocity is not the speed of light but is given by the speed of sound (or second sound in the case of superfluid helium). However, a more detailed picture of defect formation is as follows: Any continuous phase transition is dominated by critical fluctuations. Approaching T_c from above, ordered (but fluctuating in time) domains get larger and larger, and order-parameter correlation functions diverge algebraically, free of any typical length scale. Since the critical exponent above and below T_c is the same, the divergence is symmetric. It follows that the structure of ordered domains above T_c appears mirrored to disordered regions below T_c, like a negative image. Exactly at T_c, the correlation length is infinite, and the structure is self-similar on all scales, showing a fractal pattern. Both ordered and disordered regions cover 50% of the volume. Since the energy difference between both phases is zero at T_c (and very small in the vicinity), the pattern is not static but fluctuates. The larger the domains, the slower they appear and disappear. Not only do length scales diverge, but also time scales: The temporal order-parameter correlation function diverges algebraically as well. This behavior in the vicinity of T_c is called critical slowing down.

For any nonzero (most easily linear) cooling rate, one can compare the critical slowing down with the time to reach the transition. Far away from the transition, correlation times are short, and order-parameter fluctuations can follow the cooling. The system is quasiadiabatic. If the correlation time becomes larger than the time to reach the transition, fluctuations can no longer follow, and a fingerprint of the longest length scale is taken. This well-defined fallout time defines the largest

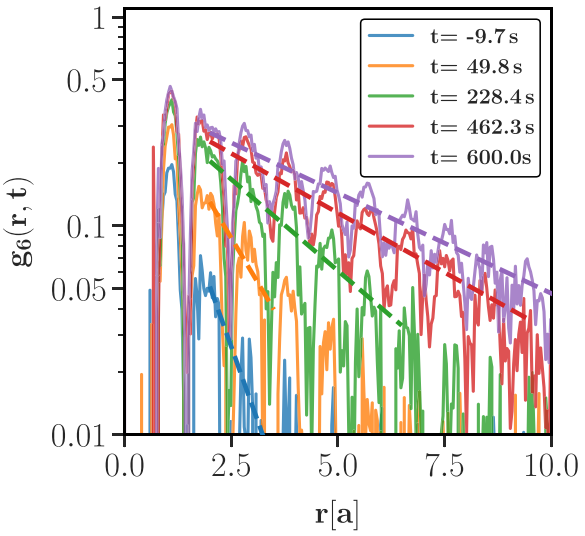

FIG. 1. Bond order correlation function before the quench (blue) at an initial $\Gamma_{\text{In}} = 16$ and after to a final coupling strength of $\Gamma_F = 74$ for various waiting times. Dotted lines are exponential fits to the curves, which appear as straight lines in the lin-log plot.

size of the symmetry-broken domains (SBDs) for the given cooling rate. Why the scenario of Kibble and Zurek yields the same result was recently calculated by F. Suzuki and W. Zurek explicitly for the Ginzburg-Landau model [19]:

$$\hat{\xi} = \xi_0 \left(\frac{\tau_Q}{\tau_0} \right)^{\frac{\nu}{1+\nu z}}, \tag{1}$$

with $\hat{\xi}$ being the domain size, ν and z critical exponents, and τ_Q the quench time. Many systems have been investigated to test the Kibble-Zurek mechanism, e.g., in liquid crystals [20], superfluid ^{3}He [21], superconducting systems [22], convective, intrinsically out-of-equilibrium systems [23], multiferroics [24], quantum systems [25], ion crystals [26,27], and Bose-Einstein condensates [28] (the latter two systems contain the effect of inhomogeneities due to, e.g., temperature gradients). A detailed review concerning the significance and limitations of these experiments can be found in Refs. [14,29]. Recent work includes quantum systems also in two dimensions [30–32], and universal behavior as well as limitations of the Kibble-Zurek scaling is discussed in Refs. [33,34]. For the 2D and 3D Ising models, zero-temperature quenches are reported in Refs. [35,36], including the growth exponents. In classical two-dimensional ensembles and for linear cooling rates, the Kibble-Zurek scaling was proven to be valid also for the Kosterlitz-Thouless universality [37].

Here, we go beyond the Kibble-Zurek picture and cool the ensemble on timescales where τ_Q is effectively zero. The monolayer has a two-component order parameter ($2N$) given by the director field of nearest neighbors. This property is shared by the Higgs field and superfluid helium, apart from the fact that the latter is a complex quantity. Since the ensemble is two dimensional and consists of micrometer-sized particles, defects and domains can be monitored *in situ* by video microscopy, unlike in three-dimensional ensembles, where typically only the surface of the bulk can be monitored.

The experiment in detail is described in Ref. [38], and it was successful in validating 2D melting theory [39–41]. Here, only a brief description is given: In a droplet of a suspension composed of superparamagnetic polystyrene spheres [42], particles are dispersed in a water droplet, which is suspended by surface tension in a top-sealed cylindrical hole ($\varnothing = 6\,\mathrm{mm}$) of a glass plate. The particles are 4.5 µm in diameter and have a mass density of $1.5\,\mathrm{g/cm^3}$, leading to sedimentation. The large density is due to the fact that the polystyrene beads are doped with iron oxide nanoparticles, which further cause the superparamagnetic behavior. After sedimentation, particles are arranged in a monolayer at the water-air interface of the droplet. The interface is kept planar (less than 250 nm height difference from the center to the border) by active regulation based on several control loops using digital image analysis. It is kept horizontal, with changes in inclination of less than 1 mrad, by an inclination sensor driving a tripod on which the whole setup is mounted. In this way, the ensemble forms an ideal two-dimensional system, without any pinning of particles to the substrate. The particles themselves are small enough to perform 2D Brownian motion but large enough to be monitored by video microscopy. The positions of the particles are analyzed using the software package of Crocker and Grier [43]. The field of view of the video camera is $1160 \times 865\,\mu\mathrm{m}^2$ in size and contains about 9000 colloids, while the whole monolayer contains approximately 300 000 particles. An external magnetic field H, perpendicular to the water-air interface, induces a magnetic moment in each bead (parallel to the applied field), leading to repulsive dipole-dipole interactions between all particles. We use the dimensionless control parameter Γ to characterize this interaction strength. Γ is given by the ratio of dipolar magnetic energy to thermal energy:

$$\Gamma = \frac{\mu_0}{4\pi}\frac{(\chi H)^2(\pi\rho)^{3/2}}{k_B T} \propto T_{\mathrm{sys}}^{-1}, \tag{2}$$

and thus can be regarded as a dimensionless inverse system temperature or a dimensionless in-plane pressure. The state of the system in thermal equilibrium—liquid, hexatic, or solid—is solely defined by the strength of the magnetic field H, since the laboratory temperature T, the two-dimensional particle density ρ, and the magnetic susceptibility per bead χ are kept constant experimentally.

In these units, the transition (crystalline-hexatic) is at $\Gamma_m = 70 \pm 0.5$ and the transition from hexatic to isotropic at about $\Gamma_i = 68 \pm 0.5$ [44]. Since the system temperature is given by an outer field, enormously high cooling rates are accessible compared to atomic systems. Based on a well-equilibrated liquid system with an initial interaction strength at $\Gamma_{\mathrm{In}} \approx 16$, deep in the fluid phase, we initiate a temperature jump with cooling rates up to $d\Gamma/dt \approx 10^4\ \mathrm{s}^{-1}$ into the crystalline region of the phase diagram $\Gamma_F \geqslant 70$. This temperature quench triggers solidification within the whole monolayer. The cooling timescale is 10^5 times faster compared to the fastest intrinsic time, given, e.g., by the Brownian time $\tau_B = 50\,\mathrm{s}$, which is the time a particle needs to diffuse the distance of its own diameter. In atomic systems, this timescale is much faster (Brownian time in water is $\sim 10^{-11}$ s); thus, comparable rates are rarely accessible.

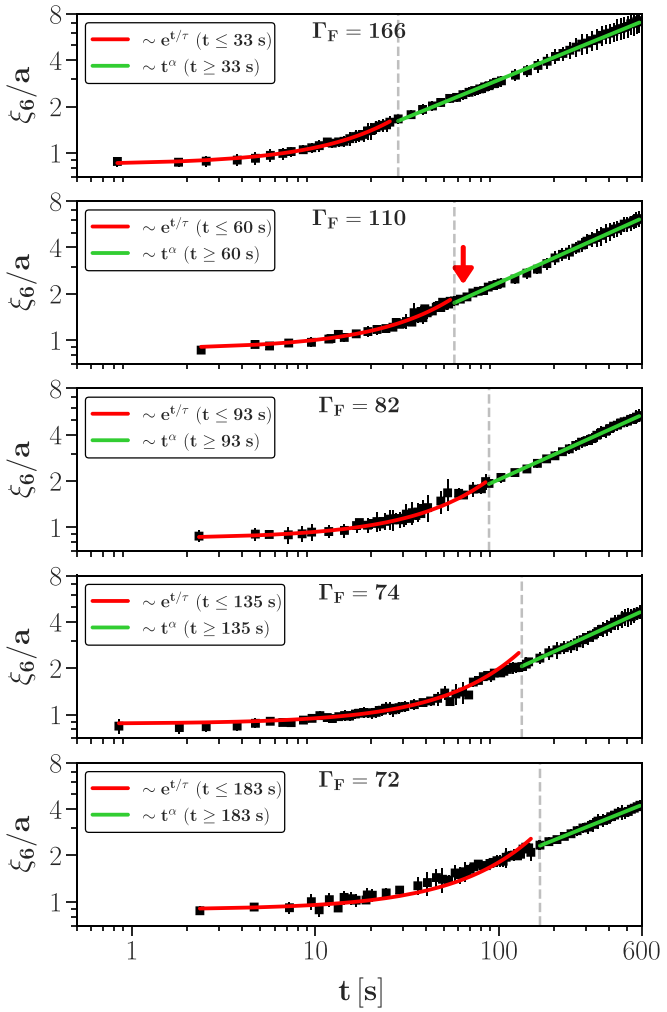

FIG. 2. ξ_6 is presented in a log-log plot for different quench depths. Shortly after the quench, the growing behavior is exponential and switches to algebraic later. The quench depth increases from bottom to top and the crossover time decreases for deeper quenches. The crossover from exponential to algebraic takes place when about 37% particles belong to symmetry-broken domains (see discussion below). The vertical dashed lines are the times, where the number of domains have their maximum, indicated with arrows in Fig. 4. For the quench $\Gamma_F = 110$, the red arrow shows the time that the system is in the state shown in Fig. 3.

A further enormous advantage of the two-dimensional ensemble is that there is no heat flux through the bulk, and especially through the surface of the material, as is usually the case in 3D condensed matter systems. At extreme cooling rates, this would easily lead to temperature or pressure gradients, causing an inhomogeneous background during symmetry breaking. This is ruled out in our experiment. To increase statistics, each temperature quench is repeated at least 10 times to the same designated final value of the control parameter Γ_F, with sufficient equilibration times in between.

II. RESULTS

A. Orientational correlations

Ordering in 2D is best measured with the sixfold bond order correlation function $g_6(r)$, since the close-packed crystal

structure in 2D is always hexagonal, at least for isotropic interactions of the particles:

$$g_6(r) = \langle|\psi(\vec{r}_k)\psi^*(\vec{r}_j)|\rangle_{kj} = \langle|\psi(\vec{r})\psi^*(\vec{0})|\rangle. \quad (3)$$

$g_6(r)$ is based on the local director field given by the nearest neighbors. For a particle numbered with l, it reads $\psi_l = 1/N_j \sum_{k=1}^{N_j} e^{i6\theta_{kl}}$. Here, N_j counts the nearest neighbors that define the bond directions θ_{kl} with respect to a fixed but arbitrary axis. Figure 1 shows the bond order correlation function $g_6(r,t)$ for various times: The lowest (blue) curve is before the quench, and the other four curves are after the quench. To characterize the decay, we plot the data in a semilogarithmic plot: For all times, it decays exponentially, and no signature of algebraic decay is detectable as observed in equilibrium measurements. Thus, the orientational order is always short range, and no quasi-long-range order appears, ruling out signatures of a hexatic phase, which are prominent in 2D melting in equilibrium [39].

From the exponential decay $g_6(r,t) \sim \exp(-r/\xi_6(t))$ of the bond order correlation length (Fig. 1), one can extract the orientational correlation length $\xi_6(t)$ as a function of time for different quench rates. As shown in Fig. 2, the correlation length always grows monotonically after the quench. This is true for low quenches ($\Gamma_F = 72$ and 74), intermediate quenches ($\Gamma_F = 80$ and 110), and deep quenches ($\Gamma_F = 166$). In the Supplemental Material [45], we show that two other length scales (1) extracted from the standard pair correlation function and (2) the length given by the inverse defect density give qualitatively identical results. The black squares are the correlation length as a function of time, averaged over about ten quenches from $\Gamma_{\text{In}} = 16$ for each final interaction strength Γ_F, and the error bar represents the standard deviation of the mean. In the early stage, we observe a nonalgebraic growth of the domain size (red curves), followed by an algebraic one (green curves) for all quenches. The nonalgebraic time window is best fitted with an exponential increase of the bond order correlation length, as checked by the goodness-of-fit statistic.

B. Determining symmetry-broken domains

Measuring crystallinity on a local scale in 2D is not trivial: Mermin-Wagner-Hohenberg fluctuations [46–48] preclude perfect long-range translational order, and hence it rules out the use of positional order. Furthermore, orientational order has always to be compared with the local neighborhood. An elaborate discussion of how to define symmetry-broken domains in 2D can be found in Ref. [49]. We define a particle to be part of a symmetry-broken domain if the following three conditions are fulfilled for the particle itself and at least one nearest neighbor:

(1) The magnitude of the local bond order field m_{6_k} must exceed 0.6 for both neighboring particles.

(2) The bond length deviation $\Delta|l_{kl}|$ of neighboring particles k and l is less than 10% of the average particle distance l_a.

(3) The variation in bond orientation $\Delta\Theta = |\psi_k - \psi_l|$ of neighboring particles k and l must be less than 2.3° in real space (less than 14° in sixfold space).

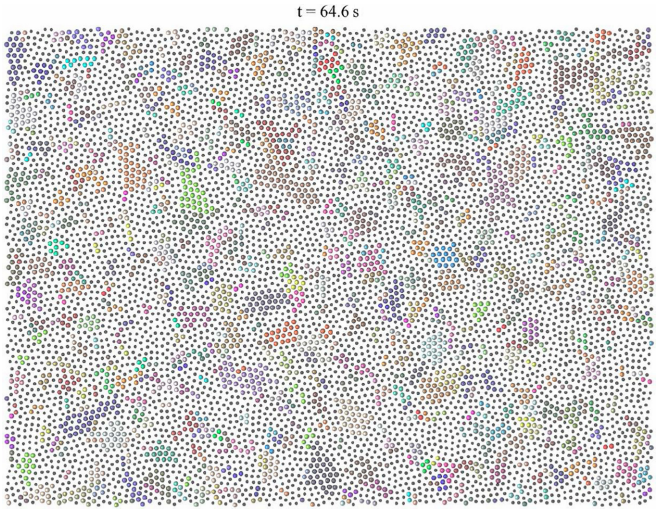

FIG. 3. The symmetry-broken domains are presented 64 s after a quench from $\Gamma_{\text{In}} = 16$ to a final coupling strength of $\Gamma_F = 110$. Small dots are fluidlike particles, whereas big ones are crystal-like. Different colors indicate individual grains, which are labeled in time.

Simply connected clusters of particles that fulfill all three criteria are merged into a local symmetry-broken domain. Figure 3 shows a snapshot of the ensemble with local domains marked in different colors, while particles still in a high-symmetry configuration are plotted as small gray dots. The parameters are optimized to be (1) soft enough to identify monocrystals in equilibrium with Mermin-Wagner-Hohenberg fluctuations on top and (2) sharp enough to discriminate individual domains in space and time. From this data, one can analyze the number and the size of the domains for each time step. Individual domains fluctuate strongly, and many of them dissolve again in the early period after the quench. At later times, when only grain boundaries are left as the high-symmetry phase, the domains appear stable besides grain boundary fluctuations. In the following, we analyze the number and size of domains that are completely within the field of view as a function of time after the quench.

C. Number and size of domains

Figure 4 (left) shows the average number of local domains as a function of time up to 300 s after the quench, and the inset shows the mean size. As expected, the mean size of the nuclei grows monotonically for all quench depths. The average number of domains (Fig. 4, left) first increases, but finally decreases in time, since they become larger but fewer. The maximum shifts to shorter times as a function of quench depth—deeper supercooling drives the system faster to the solid but polycrystalline state. Note that domain growth starts immediately after the quench, such that no lag time known from classical nucleation theory is detectable [5,50]. Figure 4 (right) shows the same data but plotted as a function of crystallinity X instead of time. Here, we define crystallinity X as the fraction of particles belonging to a symmetry-broken domain with respect to all particles. Interestingly, all curves almost superimpose and show universal behavior as a function of crystallinity. Surprisingly, the position and height of the

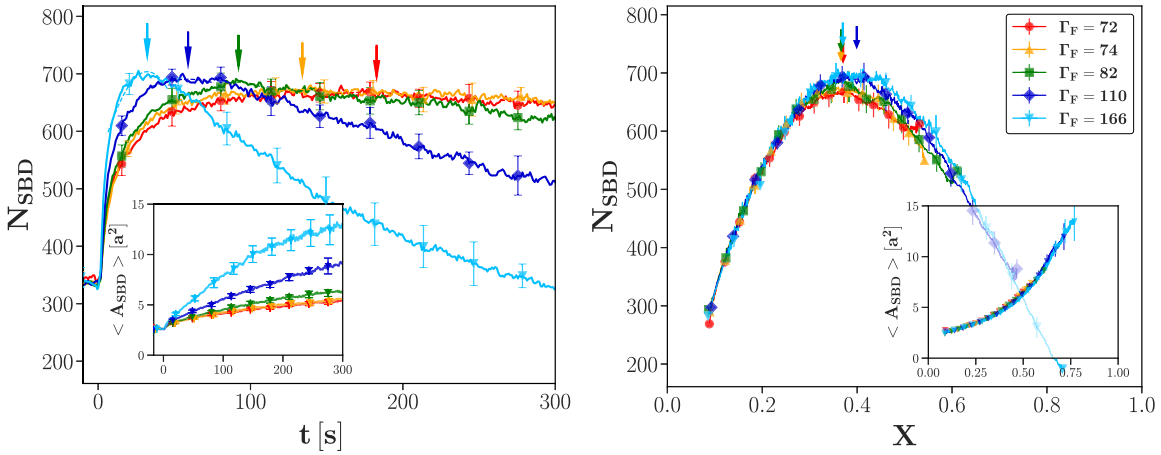

FIG. 4. The left image shows the number of symmetry-broken domains and the average size of the domains (inset) as a function of time for different quench depths. The error bars are averages of about ten independent quenches with about 9000 particles in the field of view. Whereas the average size of the symmetry-broken domains grows monotonically as expected, the number of symmetry-broken domains first increases to a maximum but then decreases in favor of fewer but larger domains. The arrows are a guide to the eye to identify the maximums extracted by fitting a Gaussian distribution around the numeric maxima of the experimental data. The right image shows the same data but plotted as the fraction of symmetry-broken area, which is implicitly a function of time. The curves almost superimpose as a function of crystallinity and are independent of the quench depth. The arrows are pointing to the maximum of each curve, which is about X $\sim$ 37%.

average number of symmetry-broken domains (in the context of nucleation, this is called the mosaicity) are independent of the quench depth. The maximum in N_{SBD} appears when a fraction of 0.37 ± 0.02 of particles belong to symmetry-broken domains. The maxima are indicated as arrows in Fig. 4. It is exactly the time we took as the crossover time separating exponential from algebraic growth in Fig. 2, indicated by the dashed vertical line. Notably, 0.37 ± 0.02, being numerically so close to the percolation threshold $n_c^* \sim 0.359$ of the 2D Lorentz model [51,52], motivates interpreting the crossover as a percolationlike phenomenon.

For different quench depths, we propose the following scenario: After a quench, local symmetry-broken domains start to grow exponentially until about 37% of the space is covered. In this time window, the ensemble is dominated by critical-like fluctuations, and most of the domains disappear again [53]. In our 2D system, the fraction of 37% crystallinity marks a threshold where domains with different orientations start to touch. From this point on, critical-like fluctuations become suppressed, and the following dynamics is dominated by the transformation of the high-symmetry phase in the residual interstices of the symmetry-broken phase. This period is marked by an algebraic increase in the bond order correlation length.

III. CONCLUSION

The paradigmatic melting theory in 2D, the Kosterlitz-Thouless-Halperin-Nelson-Young theory, starts with a highly idealized monocrystal, free of dislocations, disclinations, vacancies, interstitials, or grain boundaries. Recursion relations for elasticity, shielded by virtual dislocations, can be solved by renormalization group theory until shear elasticity disappears under heating, entering a fluid phase. However, this monocrystal can never be obtained by cooling, at least in the thermodynamic limit. The framework is given by Tom Kibble and Wojciech Zurek, who argued with causality and critical slowing down, respectively. Out of equilibrium and for any nonzero cooling rate, the ensemble will become polycrystalline with a domain size given by the cooling rate. In the thermodynamic limit, freezing and melting are not reversible, taking timescales into account.

Here, we use a monolayer of superparamagnetic colloids, which can be cooled free of gradients on unprecedentedly fast timescales compared to any intrinsic dynamics of the ensemble. We find universal behavior of the domain size and number of domains, independent of how deep we quench into the crystalline phase. This shows up most easily when the timescale is normalized by crystallinity X, the area fraction of symmetry-broken domains. This is in stark contrast to ensembles with underlying first-order transitions, where the mosaicity depends on the degree of supercooling *after* the quench, when the system is jumped between the binodal and the spinodal; forming a critical nucleus and overcoming the energy barrier is a rare event [5,50]. For weak supercooling, the barrier is less frequently overcome compared to deep supercooling. Therefore, a nucleus has more time to grow until it touches the surface of a neighboring grain. For deep supercooling, grains are less dilute in space and time, and grains have less time to grow before they touch: One finds more and smaller grains when the system is completely transformed. In both cases, there is no memory of the fluid phase before cooling—In standard classical nucleation theory, the isotropic fluid is supposed to be structureless.

For second-order phase transitions and linear cooling rates, the domain size is determined by the correlation length at the fallout time. In Fig. 4 of Ref. [37], we plotted defect density and domain sizes also for the equilibrium system (black data points), down to $\Gamma = 30$: The onset of critical behavior is detected surprisingly far away from T_c; thus, the fluid is not completely structureless. For instantaneous quenches, this tiny onset of structure is the starting point for further evolution, causing the ensemble to have a memory of where it

started. We propose that mosaicity depends on the temperature *before* the quench, and by quenching, one picks out the onset of criticality surprisingly far away from the transition.

Taking the time-dependent bond order correlation length, we can identify two regimes: first an exponential growth, followed by an algebraic one. For the Lambda transition of He^4, Zurek proposed an algebraic decrease of the inverse defect density after the quench [17]. For the *XY* model, a power-law increase of the correlation length with a small logarithmic correction is predicted due to defect annihilation [54], and in dusty plasma, a two-step process, but from algebraic to algebraic, was found experimentally [55]. We do not have a universal theory for the initial exponential growth in the colloidal ensemble—differences compared to dusty plasma may depend on specific properties like overdamped versus ballistic ensembles—but we focus on the two-step behavior. In our 2D particle ensemble, the crossover is at about 37% transformed area (= crystallinity). This coincides with the time when the number of domains starts to decrease. The microscopic picture we have in mind is as follows: In the first regime, symmetry-broken domains appear but are still strongly affected by critical-like fluctuations: Most of them disappear again. At about 37% crystallinity, symmetry-broken domains start to touch, and critical-like fluctuations are damped. This is reasonable, since the crossover agrees within the error bars with the percolation threshold in 2D. In the second regime, critical-like fluctuations play a less dominant role, fewer domains dissolve, larger ones grow more dominantly, and the total number of domains decreases.

ACKNOWLEDGMENTS

P.K. acknowledges financial support from the German Research Foundation (DFG), Projects No. 453041792 (Heisenberg funding), No. 408261333, and No. 237282255.

A.V.: formal analysis, software, investigation, validation, visualization; P.D.: data curation, formal analysis, software, investigation, validation, visualization; P.K.: conceptualization, project administration, validation, writing—original draft.

DATA AVAILABILITY

The raw data consist of positional data in 2D recorded in a binary format of idl (Integrated Data Language) based on the software package of Crocker and Grier [43] for digital image analysis. We converted one exemplary dataset to ASCII and uploaded it to the public repository [56]. The data that support the findings of this article are not publicly available. The data are available from the authors upon reasonable request.

[1] H. N. Ritland, Density phenomena in the transformation range of a borosilicate crown glass, J. Am. Ceram. Soc. **37**, 370 (1954).

[2] K. Vollmayr, W. Kob, and K. Binder, Cooling-rate effects in amorphous silica: A computer-simulation study, Phys. Rev. B **54**, 15808 (1996).

[3] C. A. Angell, K. L. Ngai, G. B. McKenna, P. F. McMillan, and S. W. Martin, Relaxation in glassforming liquids and amorphous solids, J. Appl. Phys. **88**, 3113 (2000).

[4] P. G. Debenedetti and F. H. Stillinger, Supercooled liquids and the glass transition, Nature (London) **410**, 259 (2001).

[5] K. Binder, Theory of first-order phase transitions, Rep. Prog. Phys. **50**, 783 (1987).

[6] L. Onsager, Crystal statistics. I. A two-dimensional model with an order-disorder transition, Phys. Rev. **65**, 117 (1944).

[7] J. M. Kosterlitz and D. J. Thouless, Long range order and metastability in two dimensional solids and superfluids (application of dislocation theory), J. Phys. C **5**, L124 (1972).

[8] J. M. Kosterlitz and D. J. Thouless, Ordering, metastability and phase transitions in two-dimensional systems, J. Phys. C **6**, 1181 (1973).

[9] D. R. Nelson and B. I. Halperin, Dislocation-mediated melting in two dimensions, Phys. Rev. B **19**, 2457 (1979).

[10] B. I. Halperin and D. R. Nelson, Theory of two-dimensional melting, Phys. Rev. Lett. **41**, 121 (1978).

[11] A. P. Young, Melting and the vector Coulomb gas in two dimensions, Phys. Rev. B **19**, 1855 (1979).

[12] T. W. B. Kibble, Topology of cosmic domains and strings, J. Phys. A: Math. Gen. **9**, 1387 (1976).

[13] T. W. B. Kibble, Some implications of a cosmological phase transition, Phys. Rep. **67**, 183 (1980).

[14] T. Kibble, Phase-transition dynamics in the lab and the universe, Phys. Today **60**, 47 (2007).

[15] Y. B. Zel'dovic, I. Kobzarev, and O. L.B., Cosmological consequences of a spontaneous breakdown of a discrete symmetry, Zh. Eksp. Teor. Fiz. **67**, 3 (1974).

[16] W. H. Zurek, Cosmological experiments in superfluid helium? Nature (London) **317**, 505 (1985).

[17] W. H. Zurek, Cosmic strings in laboratory superfluids and the topological remnants of other phase transitions, Acta Phys. Pol. B **24**, 1301 (1993).

[18] W. H. Zurek, Cosmological experiments in condensed matter systems, Phys. Rep. **276**, 177 (1996).

[19] F. Suzuki and W. H. Zurek, Deconstructing dynamics of symmetry breaking, Proc. Natl. Acad. Sci. USA **122**, e2523903122 (2025).

[20] I. Chuang, R. Durrer, N. Turok, and B. Yurke, Cosmology in the laboratory: Defect dynamics in liquid crystals, Science **251**, 1336 (1991).

[21] C. Bäuerle, Y. M. Bunkov, S. N. Fisher, H. Godfrin, and G. R. Pickett, Laboratory simulation of cosmic string formation in the early universe using superfluid ^{3}He, Nature (London) **382**, 332 (1996).

[22] R. Carmi, E. Polturak, and G. Koren, Observation of spontaneous flux generation in a multi-Josephson-junction loop, Phys. Rev. Lett. **84**, 4966 (2000).

[23] M. A. Miranda, J. Burguete, H. Mancini, and W. González-Viñas, Frozen dynamics and synchronization through a secondary symmetry-breaking bifurcation, Phys. Rev. E **87**, 032902 (2013).

[24] S. C. Chae, N. Lee, Y. Horibe, M. Tanimura, S. Mori, B. Gao, S. Carr, and S. W. Cheong, Direct observation of the proliferation

of ferroelectric loop domains and vortex-antivortex pairs, Phys. Rev. Lett. **108**, 167603 (2012).

[25] X.-Y. Xu, Y.-J. Han, K. Sun, J.-S. Xu, J.-S. Tang, C.-F. Li, and G.-C. Guo, Quantum simulation of Landau-Zener model dynamics supporting the Kibble-Zurek mechanism, Phys. Rev. Lett. **112**, 035701 (2014).

[26] S. Ulm, J. Roßnagel, G. Jacob, C. Degünther, S. T. Dawkins, U. G. Poschinger, R. Nigmatullin, A. Retzker, M. B. Plenio, F. Schmidt-Kaler, and K. Singer, Observation of the Kibble–Zurek scaling law for defect formation in ion crystals, Nat. Commun. **4**, 2290 (2013).

[27] K. Pyka, J. Keller, H. L. Partner, R. Nigmatullin, T. Burgermeister, D. M. Meier, K. Kuhlmann, A. Retzker, M. B. Plenio, W. H. Zurek, A. del Campo, and T. E. Mehlstäuble, Topological defect formation and spontaneous symmetry breaking in ion Coulomb crystals, Nat. Commun. **4**, 2291 (2013).

[28] G. Lamporesi, S. Donadello, S. Serafini, F. Dalfovo, and G. Ferrari, Spontaneous creation of Kibble–Zurek solitons in a Bose–Einstein condensate, Nat. Phys. **9**, 656 (2013).

[29] A. del Campo and W. H. Zurek, Universality of phase transition dynamics: Topological defects from symmetry breaking, Int. J. Mod. Phys. A **29**, 1430018 (2014).

[30] A. Keesling, A. Omran, H. Levine, H. Bernien, H. Pichler, S. Choi, R. Samajdar, S. Schwartz, P. Silvi, S. Sachdev, P. Zoller, M. Endres, M. Greiner, V. Vuletić, and M. D. Lukin, Quantum Kibble–Zurek mechanism and critical dynamics on a programmable Rydberg simulator, Nature (London) **568**, 207 (2019).

[31] S. Ebadi, T. T. Wang, H. Levine, A. Keesling, G. Semeghini, A. Omran, D. Bluvstein, R. Samajdar, H. Pichler, W. W. Ho, S. Choi, S. Sachdev, M. Greiner, V. Vuletić, and M. D. Lukin, Quantum phases of matter on a 256-atom programmable quantum simulator, Nature (London) **595**, 227 (2021).

[32] M. Schmitt, M. M. Rams, J. Dziarmaga, M. Heyl, and W. H. Zurek, Quantum phase transition dynamics in the two-dimensional transverse-field Ising model, Sci. Adv. **8**, eabl6850 (2022).

[33] A. del Campo, Universal statistics of topological defects formed in a quantum phase transition, Phys. Rev. Lett. **121**, 200601 (2018).

[34] H.-B. Zeng, C.-Y. Xia, and A. del Campo, Universal breakdown of Kibble-Zurek scaling in fast quenches across a phase transition, Phys. Rev. Lett. **130**, 060402 (2023).

[35] H. Christiansen, S. Majumder, and W. Janke, Zero-temperature coarsening in the two-dimensional long-range Ising model, Phys. Rev. E **103**, 052122 (2021).

[36] D. Gessert, H. Christiansen, and W. Janke, Aging following a zero-temperature quench in the $d = 3$ Ising model, Phys. Rev. E **109**, 044148 (2024).

[37] S. Deutschländer, P. Dillmann, G. Maret, and P. Keim, Kibble–Zurek mechanism in colloidal monolayers, Proc. Natl. Acad. Sci. USA **112**, 6925 (2015).

[38] F. Ebert, P. Dillmann, G. Maret, and P. Keim, The experimental realization of a two-dimensional colloidal model system, Rev. Sci. Inst. **80**, 083902 (2009).

[39] P. Keim, G. Maret, and H. H. von Grünberg, Frank's constant in the hexatic phase, Phys. Rev. E **75**, 031402 (2007).

[40] U. Gasser, C. Eisenmann, G. Maret, and P. Keim, Melting of crystals in two dimensions, ChemPhysChem **11**, 963 (2010).

[41] J. M. Kosterlitz, Nobel lecture: Topological defects and phase transitions, Rev. Mod. Phys. **89**, 040501 (2017).

[42] Dynabeads, 4.5 μm, http://www.dynal.no.

[43] J. C. Crocker and D. G. Grier, Methods of digital video microscopy for colloidal studies, J. Colloid Interface Sci. **179**, 298 (1996).

[44] Earlier work [39] reports lower values due to a lower magnetic susceptibility of the colloids, measured by superconducting quantum interference device. It is now more precise to determine the susceptibility by comparison of the pair correlation function in the fluid phase with computer simulations, leading to the given transition temperatures.

[45] See Supplemental Material at http://link.aps.org/supplemental/10.1103/rmd6-ll3b for two other length scales showing qualitatively identical results.

[46] N. D. Mermin and H. Wagner, Absence of ferromagnetism or antiferromagnetism in one- or two-dimensional isotropic Heisenberg models, Phys. Rev. Lett. **17**, 1133 (1966).

[47] P. Hohenberg, Existence of long-range order in 1 and 2 dimensions, Phys. Rev. **158**, 383 (1967).

[48] N. D. Mermin, Crystalline order in two dimensions, Phys. Rev. **176**, 250 (1968).

[49] P. Dillmann, G. Maret, and P. Keim, Two-dimensional colloidal systems in time-dependent magnetic fields, Eur. Phys. J. Spec. Top. **222**, 2941 (2013).

[50] U. Gasser, E. R. Weeks, A. Schofield, P. N. Pusey, and D. A. Weitz, Real space imaging of nucleation and growth in colloidal crystallization, Science **292**, 258 (2001).

[51] T. Bauer, F. Höfling, T. Munk, E. Frey, and T. Franosch, The localization transition of the two-dimensional Lorentz model, Eur. Phys. J.: Spec. Top. **189**, 103 (2010).

[52] T. Franosch, F. Höfling, T. Bauer, and E. Frey, Persistent memory for a Brownian walker in a random array of obstacles, Chem. Phys. **375**, 540 (2010).

[53] Critical-like refers to critical phenomena similar to equilibrium conditions but being out of equilibrium and nonergodic.

[54] J. Asja and F. C. Leticia, Quench dynamics of the 2D *XY* model, J. Stat. Mech. (2011) P02032.

[55] P. Hartmann, A. Douglass, J. C. Reyes, L. S. Matthews, T. W. Hyde, A. Kovacs, and Z. Donko, Crystallization dynamics of a single layer complex plasma, Phys. Rev. Lett. **105**, 115004 (2010).

[56] A. Valizadeh, Raw Data for Symmetry Breaking on Ultrafast Timescales, Edmond – the Open Research Data Repository of the Max Planck Society, 2025, https://doi.org/10.17617/3.T3VVFB.